



CHORUS

This is the accepted manuscript made available via CHORUS. The article has been published as:

Resonant Inelastic X-Ray Scattering Response of the Kitaev Honeycomb Model

Gábor B. Halász, Natalia B. Perkins, and Jeroen van den Brink

Phys. Rev. Lett. **117**, 127203 — Published 16 September 2016

DOI: [10.1103/PhysRevLett.117.127203](https://doi.org/10.1103/PhysRevLett.117.127203)

Resonant inelastic X-ray scattering response of the Kitaev honeycomb model

Gábor B. Halász,¹ Natalia B. Perkins,² and Jeroen van den Brink^{3,4}

¹*Kavli Institute for Theoretical Physics, University of California, Santa Barbara, CA 93106, USA*

²*School of Physics and Astronomy, University of Minnesota, Minneapolis, MN 55116, USA*

³*IFW Dresden, Helmholtzstrasse 20, 01069 Dresden, Germany*

⁴*Department of Physics, Harvard University, Cambridge, MA 02138, USA*

We calculate the resonant inelastic X-ray scattering (RIXS) response of the Kitaev honeycomb model, an exactly solvable quantum-spin-liquid model with fractionalized Majorana and flux excitations. We find that the fundamental RIXS channels, the spin-conserving (SC) and the non-spin-conserving (NSC) ones, do not interfere and give completely different responses. SC-RIXS picks up exclusively the Majorana sector with a pronounced momentum dispersion, whereas NSC-RIXS also creates immobile fluxes, thereby rendering the response only weakly momentum dependent, as in the spin structure factor measured by inelastic neutron scattering. RIXS can therefore pick up the fractionalized excitations of the Kitaev spin liquid separately, making it a sensitive probe to detect spin-liquid character in potential material incarnations of the Kitaev honeycomb model.

Quantum spins in a solid can, instead of ordering in a definite pattern, form a fluid type of ground state: a quantum spin liquid (QSL) [1]. Theory predicts a remarkable set of collective phenomena to occur in such QSLs, including topological ground-state degeneracy, long-range entanglement, and fractionalized excitations. Beyond their clear theoretical appeal, these exotic properties also find applications in the field of topological quantum computing [2].

The Kitaev honeycomb model is an exactly solvable yet realistic spin model with a QSL ground state [3]. Neighboring $S = 1/2$ spins $\sigma_{\mathbf{r}}^{x,y,z}$ at the sites \mathbf{r} of the honeycomb lattice are coupled via different spin components along the three bonds connected to any given site. The Hamiltonian is then

$$H_K = -J_x \sum_{\langle \mathbf{r}, \mathbf{r}' \rangle_x} \sigma_{\mathbf{r}}^x \sigma_{\mathbf{r}'}^x - J_y \sum_{\langle \mathbf{r}, \mathbf{r}' \rangle_y} \sigma_{\mathbf{r}}^y \sigma_{\mathbf{r}'}^y - J_z \sum_{\langle \mathbf{r}, \mathbf{r}' \rangle_z} \sigma_{\mathbf{r}}^z \sigma_{\mathbf{r}'}^z, \quad (1)$$

where $J_{x,y,z}$ are the coupling constants for the three types of bonds x , y , and z [see Fig. 1(a)]. Depending on $J_{x,y,z}$, the model has two distinct phases. In the gapped (gapless) phase, the ground state is a gapped (gapless) QSL. The spins fractionalize into two types of elementary excitations in both phases: Majorana fermions and emergent gauge fluxes.

From an experimental standpoint, finding a physical realization of the Kitaev honeycomb model has proven to be a challenging task. So far, three types of honeycomb systems have been proposed as candidate incarnations of H_K : the iridates α -A₂IrO₃ with A = Na or Li [4–6], the ruthenate α -RuCl₃ [7, 8], and ultracold atoms in optical lattices [9]. In the iridates and the ruthenate, however, a potential spin-liquid phase at low temperatures is preempted by magnetic order due to residual magnetic interactions beyond H_K [5, 10]. Nevertheless, since these interactions are typically small, the higher-energy excitations above the energy scale setting the magnetic order are expected to be governed by H_K [8].

Given that QSLs are inherently defined in terms of a property that they do not have (i.e., magnetic order), their experimental identification and characterization is far from obvious [1]. One potential hallmark of QSLs is the presence of fractionalized magnetic excitations. For the Kitaev spin liquid,

it has been proposed that signatures of these excitations can be observed by inelastic neutron scattering (INS) [11, 12] and by Raman scattering (RS) with visible light [13]. However, both of these methods have important limitations. In particular, neither of them can directly probe the highly dispersive gapless Majorana excitations. INS displays an overall energy gap and shows little momentum dispersion because it creates two immobile flux excitations that dominate the response. RS creates two Majorana excitations only and measures their density of states, but it is an inherently zero-momentum probe and does not provide any information on their dispersion.

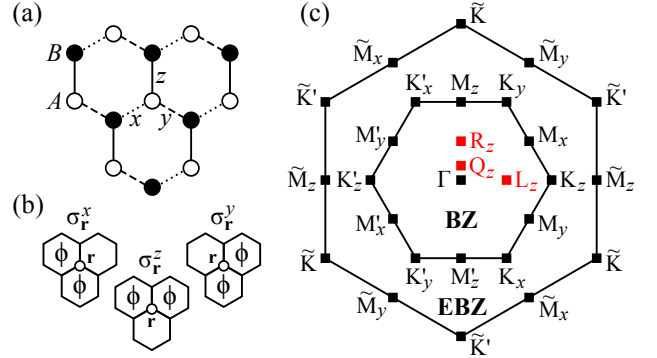


FIG. 1: (a) Illustration of the honeycomb lattice. Sites in sublattice A (B) are marked by white (black) circles, while x , y , and z bonds are marked by dotted, dashed, and solid lines, respectively. (b) Flux excitations ϕ around the photon-scattering site \mathbf{r} (white circle) in the final states $|m\rangle$ of the three fundamental NSC-RIXS channels with amplitudes $\propto \langle m | \sigma_{\mathbf{r}}^{x,y,z} e^{-it\hat{H}(\mathbf{r})} | 0 \rangle$ [see Eq. (3)], respectively. (c) Illustration of the standard Brillouin zone (BZ), and the extended Brillouin zone (EBZ) with respect to which the RIXS response is periodic. The SC-RIXS response in Fig. 3 is plotted at special points (black squares) [14] and generic representative points (red squares).

Using the exact solution of the Kitaev honeycomb model, we demonstrate in this Letter that resonant inelastic X-ray scattering (RIXS) can probe each type of fractionalized excitation directly and independently. We establish that the four fundamental RIXS channels, the spin-conserving (SC) and

the three non-spin-conserving (NSC) ones, do not interfere and give completely different responses. The SC-RIXS channel does not create any fluxes and picks up exclusively the Majorana fermions with a pronounced momentum dispersion. Conversely, the NSC-RIXS channels involve flux creation and therefore show little momentum dependence. In the physical regime, they are found to map onto the respective components of the spin structure factor measured by INS. Since the RIXS response directly quantifies both Majorana and flux excitations, it can serve as an effective probe of Kitaev-spin-liquid character in any experimental candidate material.

Formalism.—When calculating the RIXS response, we consider the L_3 -edge of the α - A_2 IrO₃ iridates with the Ir⁴⁺ ion being in a $5d^5$ configuration. However, as we later argue, our results directly translate to other edges of Ir⁴⁺ or Ru³⁺, and also to similar responses in ultracold atomic systems. RIXS is a second-order process consisting of two dipole transitions [15]. First, a photon is absorbed, and an electron from the $2p$ core shell is excited into the $5d$ valence shell, thereby creating a $2p$ core hole and an extra $5d$ electron. Second, an electron from the $5d$ valence shell decays into the $2p$ core hole, and a photon is emitted. The low-energy physics of the $5d$ electrons at each Ir⁴⁺ ion is governed by a $J = 1/2$ Kramers doublet in the t_{2g} orbitals, and we assume that $H \equiv H_K$ is the effective low-energy Hamiltonian acting on these Kramers doublets [4]. In terms of the corresponding Kitaev model, the $5d^6$ configuration in the intermediate state is then described as a vacancy or, equivalently, a non-magnetic impurity.

The initial and the final states of the RIXS process are $|0\rangle \otimes |\mathbf{Q}, \epsilon\rangle$ and $|m\rangle \otimes |\mathbf{Q}', \epsilon'\rangle$, respectively, where $|0\rangle$ is the ground state of the Kitaev model, $|m\rangle$ is a generic eigenstate with energy E_m with respect to $|0\rangle$, while \mathbf{Q} (\mathbf{Q}') is the momentum and ϵ (ϵ') is the polarization of the incident (scattered) photon. During the RIXS process, a momentum $\mathbf{q} \equiv \mathbf{Q} - \mathbf{Q}'$ and an energy $\omega = E_m$ is transferred from the photon to the Kitaev spin liquid. The total RIXS intensity is $I(\omega, \mathbf{q}) = \sum_m |\sum_{\alpha, \beta} T_{\alpha\beta} A_{\alpha\beta}(m, \mathbf{q})|^2 \delta(\omega - E_m)$, where $T_{\alpha\beta}$ is a spin-space polarization tensor depending on the microscopic details of the RIXS process (i.e., the ion type, the edge type, and the photon polarizations), and $A_{\alpha\beta}(m, \mathbf{q})$ is the scattering amplitude from $|0\rangle \otimes |\mathbf{Q}, \epsilon\rangle$ to $|m\rangle \otimes |\mathbf{Q}', \epsilon'\rangle$. This amplitude is given by the Kramers–Heisenberg formula:

$$A_{\alpha\beta}(m, \mathbf{q}) = \sum_{\mathbf{r}, \tilde{n}_{\mathbf{r}}} \frac{\langle m | d_{\mathbf{r}, \alpha} | \tilde{n}_{\mathbf{r}} \rangle \langle \tilde{n}_{\mathbf{r}} | d_{\mathbf{r}, \beta}^\dagger | 0 \rangle}{\Omega - E_{\tilde{n}} + i\Gamma} e^{i\mathbf{q} \cdot \mathbf{r}}, \quad (2)$$

where Γ is the inverse lifetime of the core hole, Ω is the energy of the incident photon with respect to the resonance energy (i.e., the energy difference between the $5d$ and the $2p$ shells), and the operator $d_{\mathbf{r}, \sigma}^\dagger$ promotes a $2p$ electron with spin σ at site \mathbf{r} into a $5d$ state at the same site. In terms of the Kitaev model, this operation is equivalent to an electron with spin $-\sigma$ being annihilated at site \mathbf{r} . The intermediate state $|\tilde{n}_{\mathbf{r}}\rangle$ is then a generic eigenstate of the Kitaev model with a single vacancy at site \mathbf{r} that has energy $E_{\tilde{n}}$ with respect to the ground state $|\tilde{0}_{\mathbf{r}}\rangle$ of the same model. Note that we use a tilde to distinguish

the model with a vacancy (intermediate states) from the one without a vacancy (initial and final states).

The four fundamental RIXS channels are introduced by decomposing the polarization tensor into $T_{\alpha\beta} = P_\eta \sigma_{\alpha\beta}^\eta$ with $\eta = \{0, x, y, z\}$, where σ^0 is the identity matrix, and $\sigma^{x,y,z}$ are the Pauli matrices. In the spin-conserving (SC) channel with $T_{\alpha\beta} \propto \sigma_{\alpha\beta}^0$, the spin of the $5d$ valence shell does not change during the RIXS process, while in the three non-spin-conserving (NSC) channels with $T_{\alpha\beta} \propto \sigma_{\alpha\beta}^{x,y,z}$, the same spin is rotated by π around the x, y, z axes, respectively. For the L_3 -edge of the Ir⁴⁺ ion, the SC coefficient is $P_0 = \epsilon^{I*} \cdot \epsilon$, while the NSC coefficients are $P_x = i(\epsilon_y^{I*} \epsilon_z - \epsilon_z^{I*} \epsilon_y)$ and $P_{y,z}$ its cyclic permutations [16].

Our first main result is that the four RIXS channels do not interfere in the case of the Kitaev model because they result in mutually orthogonal final states. In particular, the final state has no flux excitations for the SC-RIXS channel, while it has two flux excitations separated by x, y, z bonds for the three NSC-RIXS channels, respectively [see Fig. 1(b)]. We provide a detailed derivation of this result in the Supplementary Material (SM). For any scattering geometry and polarizations, the total RIXS intensity $I(\omega, \mathbf{q})$ is then a sum of four individual intensities $I_\eta(\omega, \mathbf{q}) = \sum_m |A_\eta(m, \mathbf{q})|^2 \delta(\omega - E_m)$ corresponding to the four channels $\eta = \{0, x, y, z\}$. It is derived in the SM that the individual RIXS amplitudes are

$$A_\eta(m, \mathbf{q}) \propto \sum_{\mathbf{r}} \int_0^\infty dt e^{-\Gamma t + i\Omega t + i\mathbf{q} \cdot \mathbf{r}} \langle m | \sigma_{\mathbf{r}}^\eta e^{-it\tilde{H}(\mathbf{r})} | 0 \rangle, \quad (3)$$

where $\tilde{H}(\mathbf{r}) = H + \sum_{\kappa=x,y,z} J_\kappa \sigma_{\mathbf{r}}^\kappa \sigma_{\kappa(\mathbf{r})}^\kappa$ is the Hamiltonian of the Kitaev model with a single vacancy at site \mathbf{r} . The spin at site \mathbf{r} is effectively removed from the model by being decoupled from its neighbors at sites $\kappa(\mathbf{r})$ [17].

Since the inverse lifetime Γ is by far the largest energy scale in both the iridates α - A_2 IrO₃ [18] and the ruthenate α -RuCl₃ [8, 19], we employ the fast-collision approximation to RIXS, for which $\Gamma \rightarrow \infty$ and hence $t \sim 1/\Gamma \rightarrow 0$. Expanding $e^{-it\tilde{H}(\mathbf{r})}$ up to first order in $J_{x,y,z}/\Gamma$, integrating over t , and demanding $H|0\rangle = 0$ by adding a trivial constant term to H , the RIXS amplitudes in Eq. (3) become

$$\begin{aligned} A_\eta(m, \mathbf{q}) &\propto \sum_{\mathbf{r}} e^{i\mathbf{q} \cdot \mathbf{r}} \langle m | \sigma_{\mathbf{r}}^\eta \left[1 - \frac{i\tilde{H}(\mathbf{r})}{\Gamma} \right] | 0 \rangle \\ &= \sum_{\mathbf{r}} e^{i\mathbf{q} \cdot \mathbf{r}} \langle m | \sigma_{\mathbf{r}}^\eta \left[1 - \frac{i}{\Gamma} \sum_{\kappa} J_\kappa \sigma_{\mathbf{r}}^\kappa \sigma_{\kappa(\mathbf{r})}^\kappa \right] | 0 \rangle, \end{aligned} \quad (4)$$

where we also set $\Omega = 0$ for simplicity by recognizing that its exact value does not matter as long as $\Omega \ll \Gamma$. We emphasize that the final form of Eq. (4) is expected to be generic beyond the L_3 -edge of the Ir⁴⁺ ion. For any relevant RIXS process, the couplings in the intermediate state are perturbed (i.e., weakened or switched off) around the photon-scattering site \mathbf{r} , and an analogous calculation in the fast-collision approximation would then give an identical first-order result, up to a potential renormalization of Γ .

Given that the Kitaev model is exactly solvable both in the presence and in the absence of a vacancy [17, 20], the RIXS amplitudes in Eq. (4) can be evaluated exactly. Our calculation follows the usual procedure [3]. We first take care of the static (and local) fluxes, then introduce Majorana fermions to obtain a quadratic fermion problem for each flux configuration, and finally deal with the resulting free-fermion problems by means of standard methods. However, due to technical reasons (see SM), the RIXS intensities are calculated differently for the SC and the NSC channels [21].

For the SC channel, we evaluate $A_0(m, \mathbf{q})$ for each individual final state $|m\rangle$, and obtain $I_0(\omega, \mathbf{q})$ as a histogram of $|A_0(m, \mathbf{q})|^2$ in terms of the final-state energies $\omega = E_m$. In the language of Ref. 21, this method corresponds to the few-particle approach. Indeed, it follows from Eq. (4) that, up to first order in $J_{x,y,z}/\Gamma$, there are two types of final states with a non-zero RIXS amplitude: $|m\rangle = |0\rangle$ with no excitations at all, and $|m\rangle \neq |0\rangle$ with no flux and two fermion excitations. Since scattering back into the ground state $|0\rangle$ corresponds to a purely elastic process, we restrict our attention to the $|m\rangle \neq |0\rangle$ final states with two fermion excitations at momenta \mathbf{k} and $\mathbf{q} - \mathbf{k}$. The energy of such a state is $E_m = \varepsilon_{\mathbf{k}} + \varepsilon_{\mathbf{q}-\mathbf{k}}$, where $\varepsilon_{\mathbf{k}} = 2|\lambda_{\mathbf{k}}|$ is the energy of a single fermion, and $\lambda_{\mathbf{k}} \equiv \sum_{\kappa=x,y,z} J_{\kappa} e^{i\mathbf{k}\cdot\hat{\mathbf{r}}_{\kappa}}$ in terms of the three bond vectors $\hat{\mathbf{r}}_{x,y,z}$ pointing from any site in sublattice A to its respective neighbors in sublattice B [see Fig. 1(a)]. The SC-RIXS intensity is then derived in the SM to be

$$I_0(\omega, \mathbf{q}) \propto \int_{\text{BZ}} d^2\mathbf{k} \delta(\omega - \varepsilon_{\mathbf{k}} - \varepsilon_{\mathbf{q}-\mathbf{k}}) [\varepsilon_{\mathbf{k}} - \varepsilon_{\mathbf{q}-\mathbf{k}}]^2 \times |1 - e^{i\varphi_{\mathbf{k}}} e^{i\varphi_{\mathbf{q}-\mathbf{k}}}|^2, \quad (5)$$

where $e^{i\varphi_{\mathbf{k}}} \equiv \lambda_{\mathbf{k}}/|\lambda_{\mathbf{k}}|$ is a phase factor between the two sublattices. Since the bond vectors $\hat{\mathbf{r}}_{x,y,z}$ are not lattice vectors, the intensity is not periodic with respect to the standard Brillouin zone (BZ), but with respect to the extended Brillouin zone (EBZ) illustrated in Fig. 1(c).

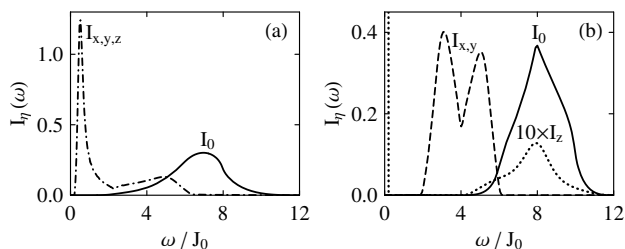


FIG. 2: Momentum-integrated RIXS intensities at (a) the isotropic point of the gapless phase [$J_{x,y,z} = J_0$] and (b) a representative point in the gapped phase [$J_{x,y} = J_0/2$ and $J_z = 2J_0$]. The SC response $I_0(\omega)$ is plotted by a solid line, while the NSC responses $I_{x,y,z}(\omega)$ are plotted by dashed and/or dotted lines. Each response is normalized such that $\int d\omega I_{\eta}(\omega) = 1$. At the gapped point, the NSC response $I_z(\omega)$ has a delta peak at low energies and is multiplied by 10 to be comparable with the other responses.

For the NSC channels, we consider the RIXS intensity directly and rewrite it as $I_{\kappa}(\omega, \mathbf{q}) \propto \int_{-\infty}^{+\infty} ds e^{i\omega s} K_{\kappa}(s, \mathbf{q})$ in terms of a time-like variable s . It is derived in the SM that the kernel of the resulting integral takes the form

$$K_{\kappa}(s, \mathbf{q}) = \langle 0 | \left[\sigma_{\mathbf{0}}^{\kappa} e^{i\tilde{H}(\mathbf{0})/\Gamma} + \sigma_{\hat{\mathbf{r}}_{\kappa}}^{\kappa} e^{i\tilde{H}(\hat{\mathbf{r}}_{\kappa})/\Gamma - i\mathbf{q}\cdot\hat{\mathbf{r}}_{\kappa}} \right] e^{-isH} \times \left[\sigma_{\mathbf{0}}^{\kappa} e^{-i\tilde{H}(\mathbf{0})/\Gamma} + \sigma_{\hat{\mathbf{r}}_{\kappa}}^{\kappa} e^{-i\tilde{H}(\hat{\mathbf{r}}_{\kappa})/\Gamma + i\mathbf{q}\cdot\hat{\mathbf{r}}_{\kappa}} \right] | 0 \rangle,$$

where $\mathbf{0}$ is any site in sublattice A . In the language of Ref. 21, this method corresponds to the determinant approach. Indeed, the ground-state expectation values in $K_{\kappa}(s, \mathbf{q})$ can be evaluated as functional determinants (see SM). We remark that the NSC-RIXS response $I_{\kappa}(\omega, \mathbf{q})$ reduces to the corresponding component κ of the spin structure factor [12] in the limit of $\Gamma \rightarrow \infty$. This result is in contrast with SC-RIXS, where the inelastic response disappears in the same limit.

Results.—We first discuss the momentum-integrated RIXS intensities $I_{\eta}(\omega) = \int_{\text{EBZ}} d^2\mathbf{q} I_{\eta}(\omega, \mathbf{q})$. In Fig. 2, the SC and NSC responses are plotted for representative points of both the gapless (a) and the gapped (b) phases. All of our responses are universal in the sense that their functional forms do not depend on the precise value of $\Gamma \gg J_{x,y,z}$. Also, some or all of the NSC responses can be identical due to symmetry. Since the maximal fermion energy is $2 \sum_{\kappa} J_{\kappa} = 6J_0$ at both representative points, the responses with maximal energies $\approx 6J_0$ and $\approx 12J_0$ can be identified as predominantly one-fermion and two-fermion responses, respectively [21]. Similarly, any delta peak close to zero energy corresponds to a zero-fermion response. Unlike the NSC responses, the SC response is always dominated by two-fermion excitations. Furthermore, the SC and NSC responses have different low-energy behavior in the gapless phase. The NSC response has an energy gap due to flux creation, while the SC response is found to vanish as $\propto \omega^5$ in the limit of $\omega \rightarrow 0$. Three powers of ω come from the two-fermion density of states around the Dirac points [22], and two further powers appear due to the factor $[\varepsilon_{\mathbf{k}} - \varepsilon_{\mathbf{q}-\mathbf{k}}]^2$ in Eq. (5), which indicates that the fermions at lower energies are perturbed less by the presence of the vacancy [23].

The differences between the SC and NSC responses become even more evident when we consider the momentum-resolved RIXS intensities $I_{\eta}(\omega, \mathbf{q})$. In Fig. 3, the SC response is plotted for the representative points of the two phases. The fractionalized nature of the excitations is indicated by the lack of delta peaks corresponding to well-defined $\omega(\mathbf{q})$ dispersions in the spectrum. Nevertheless, the response has a pronounced momentum dependence and is therefore able to probe the dispersions of the individual excitations directly. For example, in the gapless phase, the Dirac points K in the fermion dispersion manifest themselves in gapless responses around the Γ , K , and \tilde{K} points of the EBZ. However, the response actually vanishes at the Γ and \tilde{K} points due to the factor $[\varepsilon_{\mathbf{k}} - \varepsilon_{\mathbf{q}-\mathbf{k}}]^2$ in Eq. (5) and the fermion dispersion being symmetric around these points. There is a further depression of the response around the Γ point due to a destructive interference between the two sublattices, as indicated by the minus sign in the factor

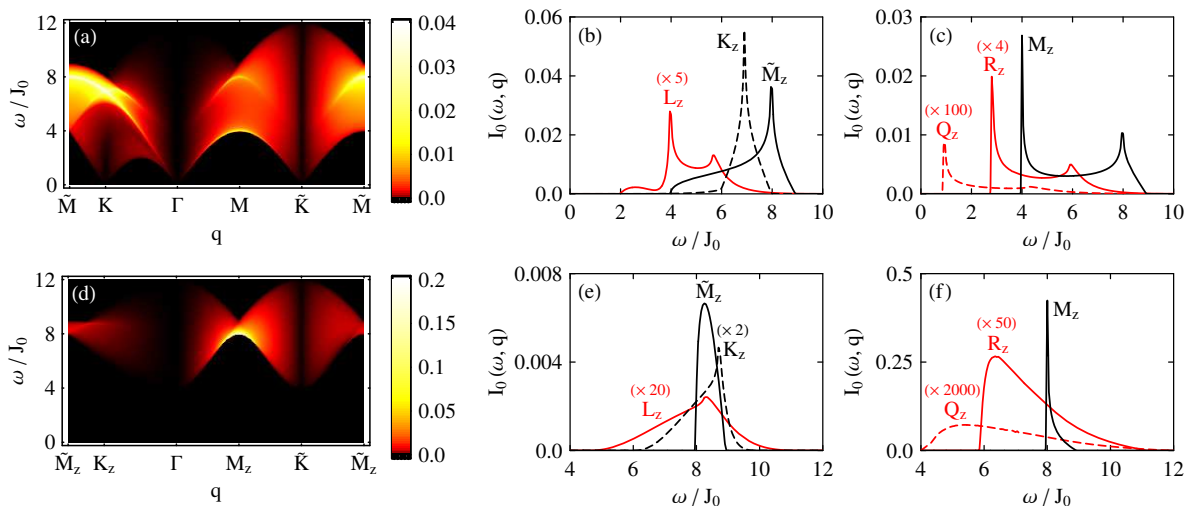


FIG. 3: Momentum-resolved SC-RIXS intensities at the isotropic point of the gapless phase [$J_{x,y,z} = J_0$] (a, b, c) and at a representative point in the gapped phase [$J_{x,y} = J_0/2$ and $J_z = 2J_0$] (d, e, f). The response is plotted along the entire \tilde{M}_z - K_z - Γ - M_z - \tilde{K} - \tilde{M}_z cut (a, d), at specific points on the Γ - K_z - \tilde{M}_z cut (b, e), and at specific points on the Γ - M_z cut (c, f) [see Fig. 1(c)]. The intensity is normalized such that $\int d\omega \int d^2\mathbf{q} I_0(\omega, \mathbf{q}) = 1$, where \mathbf{q} is measured in units of $a^{-1} \equiv |\hat{\mathbf{r}}_{x,y,z}|^{-1}$ and is integrated over the entire EBZ. Some responses are multiplied by numerical factors (written next to them) to be comparable with other responses.

$|1 - e^{i\varphi_{\mathbf{k}}} e^{i\varphi_{\mathbf{q}-\mathbf{k}}}|^2$ of Eq. (5). This effect arises because the fermions transform projectively under inversion and is therefore a direct signature of their fractionalized nature [24]. We also remark that, unlike the NSC responses, the SC response is invariant under $J_{x,y,z} \rightarrow -J_{x,y,z}$.

In contrast to the SC response, the NSC responses show little momentum dependence because the localized fluxes created by them can absorb momentum well. In fact, we find that the three NSC-RIXS components are virtually indistinguishable from the corresponding components of the spin structure factor [12] in the $\Gamma/J_0 \gtrsim 100$ regime, which is physically relevant for both α - A_2IrO_3 [18] and α - RuCl_3 [8, 19]. NSC-RIXS can therefore fully determine the spin structure factor in the iridates, for which INS is challenging due to the large neutron-absorption cross section of iridium. Although RIXS is currently limited by its energy resolution $\Delta\omega \sim J_0$ [25], this technique has been improving rapidly, and therefore $\Delta\omega \ll J_0$ is a distinct possibility for the near future.

We finally discuss the RIXS responses at a generic point of the Kitaev-spin-liquid phase, which corresponds to a generic time-reversal-invariant perturbation with respect to H_K . For the NSC-RIXS channels, the results in Ref. 22 are directly applicable and imply that the response is generically gapless. For the SC-RIXS channel, a similar analysis indicates that the response no longer vanishes at the Γ and \tilde{K} points and that $I_0(\omega)$ takes the low-energy form of $\propto \omega^3$ instead of $\propto \omega^5$ in the most generic case. However, since the characteristic lower edge of the spectrum in Fig. 3 is robust, we expect that SC-RIXS remains an effective probe of the fermion dispersion for a generic Kitaev spin liquid. Furthermore, some higher-energy features are believed to persist even beyond the phase transition into the magnetically ordered phase [8].

Conclusions.—Calculating the exact RIXS response of the Kitaev honeycomb model, we have found that the four fundamental RIXS channels, the SC and the three NSC ones, do not interfere and correspond to completely different responses. In the physically relevant regime, the SC response displays a pronounced momentum dependence and picks up the gapless Majorana fermions, while the NSC responses are only weakly momentum dependent and recover the respective components of the spin structure factor. We therefore believe that RIXS can serve as an effective probe of spin-liquid character in present and future candidate materials for the realization of the Kitaev honeycomb model.

We thank D. A. Abanin, J. T. Chalker, D. V. Efremov, and I. Rousochatzakis for useful discussions. G.B.H. is supported by a fellowship from the Gordon and Betty Moore Foundation (Grant 4304). N.P. is supported by the NSF grant DMR-1511768. J.v.d.B. acknowledges support from the Deutsche Forschungsgemeinschaft via SFB 1143 and the Harvard-MIT CUA. This research was supported in part by the National Science Foundation under Grant No. NSF PHY11-25915.

-
- [1] L. Balents, *Nature* **464**, 199 (2010); L. Savary and L. Balents, arXiv:1601.03742.
 - [2] C. Nayak, S. H. Simon, A. Stern, M. Freedman, and S. Das Sarma, *Rev. Mod. Phys.* **80**, 1083 (2008).
 - [3] A. Y. Kitaev, *Ann. Phys.* **321**, 2 (2006).
 - [4] G. Jackeli and G. Khaliullin, *Phys. Rev. Lett.* **102**, 017205 (2009).
 - [5] J. Chaloupka, G. Jackeli, and G. Khaliullin, *Phys. Rev. Lett.* **105**, 027204 (2010); J. Chaloupka, G. Jackeli, G. Khaliullin,

- Phys. Rev. Lett. **110**, 097204 (2013).
- [6] Y. Singh and P. Gegenwart, Phys. Rev. B **82**, 064412 (2010); X. Liu, T. Berlijn, W.-G. Yin, W. Ku, A. Tsvelik, Y.-J. Kim, H. Gretarsson, Y. Singh, P. Gegenwart, and J. P. Hill, Phys. Rev. B **83**, 220403(R) (2011); Y. Singh, S. Manni, J. Reuther, T. Berlijn, R. Thomale, W. Ku, S. Trebst, and P. Gegenwart, Phys. Rev. Lett. **108**, 127203 (2012); S. K. Choi, R. Coldea, A. N. Kolmogorov, T. Lancaster, I. I. Mazin, S. J. Blundell, P. G. Radaelli, Y. Singh, P. Gegenwart, K. R. Choi, S.-W. Cheong, P. J. Baker, C. Stock, and J. Taylor, Phys. Rev. Lett. **108**, 127204 (2012); F. Ye, S. Chi, H. Cao, B. C. Chakoumakos, J. A. Fernandez-Baca, R. Custelcean, T. F. Qi, O. B. Korneta, and G. Cao, Phys. Rev. B **85**, 180403(R) (2012); R. Comin, G. Levy, B. Ludbrook, Z.-H. Zhu, C. N. Veenstra, J. A. Rosen, Y. Singh, P. Gegenwart, D. Stricker, J. N. Hancock, D. van der Marel, I. S. Elfimov, and A. Damascelli, Phys. Rev. Lett. **109**, 266406 (2012).
- [7] K. W. Plumb, J. P. Clancy, L. J. Sandilands, V. V. Shankar, Y. F. Hu, K. S. Burch, H.-Y. Kee, and Y.-J. Kim, Phys. Rev. B **90**, 041112(R) (2014); L. J. Sandilands, Y. Tian, K. W. Plumb, Y.-J. Kim, and K. S. Burch, Phys. Rev. Lett. **114**, 147201 (2015); J. A. Sears, M. Songvilay, K. W. Plumb, J. P. Clancy, Y. Qiu, Y. Zhao, D. Parshall, and Y.-J. Kim, Phys. Rev. B **91**, 144420 (2015); R. D. Johnson, S. C. Williams, A. A. Haghighirad, J. Singleton, V. Zapf, P. Manuel, I. I. Mazin, Y. Li, H. O. Jeschke, R. Valentí, and R. Coldea, Phys. Rev. B **92**, 235119 (2015); L. J. Sandilands, Y. Tian, A. A. Reijnders, H.-S. Kim, K. W. Plumb, Y.-J. Kim, H.-Y. Kee, and K. S. Burch, Phys. Rev. B **93**, 075144 (2016).
- [8] A. Banerjee, C. A. Bridges, J.-Q. Yan, A. A. Aczel, L. Li, M. B. Stone, G. E. Granroth, M. D. Lumsden, Y. Yiu, J. Knolle, S. Bhattacharjee, D. L. Kovrizhin, R. Moessner, D. A. Tennant, D. G. Mandrus, and S. E. Nagler, Nat. Mater., doi:10.1038/nmat4604 (2016).
- [9] L.-M. Duan, E. Demler, and M. D. Lukin, Phys. Rev. Lett. **91**, 090402 (2003).
- [10] J. G. Rau, E. K.-H. Lee, and H.-Y. Kee, Phys. Rev. Lett. **112**, 077204 (2014); Y. Yamaji, Y. Nomura, M. Kurita, R. Arita, and M. Imada, Phys. Rev. Lett. **113**, 107201 (2014); Y. Sizyuk, C. Price, P. Wölfle, and N. B. Perkins, Phys. Rev. B **90**, 155126 (2014); I. Rousochatzakis, J. Reuther, R. Thomale, S. Rachel, and N. B. Perkins, Phys. Rev. X **5**, 041035 (2015); S. M. Winter, Y. Li, H. O. Jeschke, and R. Valentí, Phys. Rev. B **93**, 214431 (2016).
- [11] G. Baskaran, S. Mandal, and R. Shankar, Phys. Rev. Lett. **98**, 247201 (2007).
- [12] J. Knolle, D. L. Kovrizhin, J. T. Chalker, and R. Moessner, Phys. Rev. Lett. **112**, 207203 (2014).
- [13] J. Knolle, G.-W. Chern, D. L. Kovrizhin, R. Moessner, and N. B. Perkins, Phys. Rev. Lett. **113**, 187201 (2014).
- [14] Special points with and without dashes are related by inversion and have identical responses for all $J_{x,y,z}$, while those with different x, y, z subscripts are related by threefold rotation and only have identical responses when $J_x = J_y = J_z$.
- [15] L. J. P. Ament, M. van Veenendaal, T. P. Devereaux, J. P. Hill, and J. van den Brink, Rev. Mod. Phys. **83**, 705 (2011); L. Savary and T. Senthil, arXiv:1506.04752.
- [16] L. J. P. Ament, G. Khaliullin, and J. van den Brink, Phys. Rev. B **84**, 020403(R) (2011).
- [17] G. B. Halász, J. T. Chalker, and R. Moessner, Phys. Rev. B **90**, 035145 (2014).
- [18] J. P. Clancy, N. Chen, C. Y. Kim, W. F. Chen, K. W. Plumb, B. C. Jeon, T. W. Noh, and Y.-J. Kim, Phys. Rev. B **86**, 195131 (2012); V. M. Katukuri, S. Nishimoto, V. Yushankhai, A. Stoyanova, H. Kandpal, S. Choi, R. Coldea, I. Rousochatzakis, L. Hozoi, and J. van den Brink, New J. Phys. **16**, 013056 (2014).
- [19] A. Koitzsch, C. Habenicht, E. Müller, M. Knupfer, B. Büchner, H. Kandpal, J. van den Brink, D. Nowak, A. Isaeva, and T. Doert, arXiv:1603.05507; C.-H. Hsu, B.-C. Chang, Y.-F. Chen, H.-C. Ku, and H.-J. Lin, unpublished.
- [20] A. J. Willans, J. T. Chalker, and R. Moessner, Phys. Rev. Lett. **104**, 237203 (2010); A. J. Willans, J. T. Chalker, and R. Moessner, Phys. Rev. B **84**, 115146 (2011).
- [21] J. Knolle, D. L. Kovrizhin, J. T. Chalker, and R. Moessner, Phys. Rev. B **92**, 115127 (2015).
- [22] X.-Y. Song, Y.-Z. You, and L. Balents, arXiv:1604.04365.
- [23] G. B. Halász and J. T. Chalker, in preparation.
- [24] Y.-Z. You, I. Kimchi, and A. Vishwanath, Phys. Rev. B **86**, 085145 (2012).
- [25] H. Gretarsson, J. P. Clancy, Y. Singh, P. Gegenwart, J. P. Hill, J. Kim, M. H. Upton, A. H. Said, D. Casa, T. Gog, and Y.-J. Kim, Phys. Rev. B **87**, 220407(R) (2013); B. J. Kim, private communication.